Three-Dimensional Coherent X-Ray Diffraction Imaging of a Ceramic Nanofoam: Determination of Structural Deformation Mechanisms

A. Barty,[1] S. Marchesini,[1,2,3,*] H. N. Chapman,[1,3] C. Cui,[2] M. R. Howells,[2] D. A. Shapiro,[2] A. M. Minor,[2] J. C. H. Spence,[4] U. Weierstall,[4] J. Ilavsky,[5] A. Noy,[1] S. P. Hau-Riege,[1] A. B. Artyukhin,[1] T. Baumann,[1] T. Willey,[1] J. Stolken,[1] T. van Buuren,[1] and J. H. Kinney[6]

[1]*Lawrence Livermore National Laboratory, 7000 East Avenue, Livermore, California 94550, USA*
[2]*Lawrence Berkeley National Laboratory, 1 Cyclotron Road, Berkeley, California 94720, USA*
[3]*Center for Biophotonics Science and Technology, University of California, Davis, 2700 Stockton Boulevard, Suite 1400, Sacramento, California 95817, USA*
[4]*Department of Physics and Astronomy, Arizona State University, Tempe, Arizona 85287-1504, USA*
[5]*Advanced Photon Source, Argonne National Laboratory, Argonne, Illinois 60439, USA*
[6]*Department of Preventive and Restorative Dental Sciences, University of California, San Francisco, California 94143, USA*

(Received 31 August 2007; revised manuscript received 29 April 2008; published 28 July 2008)

Ultralow density polymers, metals, and ceramic nanofoams are valued for their high strength-to-weight ratio, high surface area, and insulating properties ascribed to their structural geometry. We obtain the labrynthine internal structure of a tantalum oxide nanofoam by x-ray diffractive imaging. Finite-element analysis from the structure reveals mechanical properties consistent with bulk samples and with a diffusion-limited cluster aggregation model, while excess mass on the nodes discounts the dangling fragments hypothesis of percolation theory.

DOI: 10.1103/PhysRevLett.101.055501 PACS numbers: 61.05.cf, 42.30.Rx, 68.37.Yz, 82.70.Rr

The topology, fractal index, stability, and structure of foams have fascinated scientists and mathematicians for decades. Foams arise in fields as diverse as cosmology (in Hawking's theory), geology, surfactants, phospholipids, cells, bone structure, polymers, and structural materials wherever lightness and strength are needed. Especially important are applications of periodic foam network theory to predictions of the structure of mesoporous crystalline materials suitable for use as catalysts [1] for cleaner fuels, and the study of the diffusion of water and oil in porous rocks. Here the rate-limiting step for diffusion is limited by the smallest pore, normally too small to be observed internally by any conventional tomographic microscopy. Aerogels are an important example of such a class of material. Described variously as ''frozen smoke'' and ''San Francisco fog,'' these terms do not refer to a particular substance itself but rather to a structural geometry a substance can assume. Many aerogels, for example, demonstrate astonishing mechanical, thermal, catalytic, and optical properties, which are ascribed to their low density and porous structure [2]. However, to date there have been few if any methods developed for ''seeing inside'' these foams in order to make an experimental determination of topology and structure at the mesoscopic length scale.

Although electron microscopy has provided the crystallinity and morphology of individual beam elements comprising the foam, no existing technique has been able to capture the three-dimensional bulk lattice arrangement over micron-scale sample dimensions. X rays provide the penetration, lacking to electrons, which allow us to study three-dimensional structure over thicknesses of micrometers. Current state-of-the art zone plate microscopes achieve a transverse spatial resolution of ≈ 15 nm half-pitch (30 nm period) [3], but have difficulty sustaining this resolution through the bulk structure of micron-sized three-dimensional objects due to depth of focus limitations.

We report here a three-dimensional structure determination at the mesoporous length scale ($\approx$15 nm) of a micron-sized fragment of aerogel obtained by inversion of coherent x-ray diffraction patterns [4]. The complexity of the structure observed is far greater than that of samples previously studied by this technique, and was made possible by advances in computational phase retrieval methods, the addition of holographic reference points near the specimen, and by the inherent sparsity of the foam. More generally, we demonstrate the ability of diffraction imaging to image an unknown, isolated object at high resolution in three dimensions, opening the door to a wide range of applications in material science, nanotechnology, and cellular biology.

The aerogel sample imaged here is a low density (100 mg/cm^{-3}, 1.2% bulk density) high-Z Ta_2O_5 metal oxide nanofoam, chosen because of its potential use in double shell laser ignition targets for fusion (which require a very low density material with high Z) and because of its stability under an intense x-ray beam. Because the strength of these ultralow density foams is orders of magnitude less than expected, it is important to understand and identify the unique microstructures of these foams, and to relate them to the bulk physical properties. Using the structure observed as a high-fidelity template for finite-element analysis, we calculate the load displacement response of the foam, and compare the resulting stiffness against various structural models.

X-ray diffraction imaging is elegant in its experimental simplicity: a monochromatic and coherent x-ray beam illuminates the sample, and the far-field diffraction pattern from the object is recorded on an area detector (Fig. 1). Multiple orientations fill out a three-dimensional diffraction volume, which is proportional to the Fourier transform of the object index of refraction. The detection system records only the diffracted intensities, but phase retrieval techniques can be applied to recover a three-dimensional image of the sample [5–7]. The feasibility of this technique for reconstructing an image of the sample from its diffraction pattern has been well demonstrated in many x-ray diffraction experiments [4,8–11].

A 3D implementation of the HIO algorithm [5] was used for phase reconstruction on the 3D volume with feedback parameter $\beta = 0.9$ and support refinement [6] for 1200 iterations, followed by the RAAR algorithm [6] through to iteration 3000 also with feedback parameter of $\beta = 0.9$. Missing data from both the central beamstop and inaccessible sample rotations was accounted for during phase retrieval using the SHRINKWRAP algorithm, in which the object support itself acts as a constraint in the regions of missing data [10,12]. By applying full three-dimensional phase retrieval directly to the 3D diffraction volume, as done here, we avoid the inconsistencies and image alignment problems caused by dividing the phase retrieval and tomographic data assembly into two separate steps performed sequentially [8]. Ewald sphere curvature included in the 3D data assembly avoids defocus artifacts typical of such two step reconstruction process, as well as any lens-based microtomography volume reconstruction. The phase reconstruction techniques employed here, including a detailed analysis of spatial resolution and methods for handling the limited number of views, missing angles, and central beamstop, are described in detail elsewhere [10] (see also supplemental material [13]).

The aerogel itself was prepared by a sol-gel process that involved the controlled hydrolysis of tantalum ethoxide, followed by rapid supercritical extraction of the reaction solvent [14]. The tantala aerogels obtained from this particular formulation are isolated as translucent monoliths with bulk densities of approximately 100 mg/cm^3, as determined from bulk sample mass and dimensions. We mounted an irregular 1–2 μm sized piece on a 50 nm thick rectangular silicon nitride membrane window of 2 mm $\times$ 50 μm size supported in a 200 μm thick silicon wafer frame. Several 50 nm platinum dots were placed in proximity to the sample using an electron beam to locally decompose a metal-organic precursor gas (Fig. 2). These dots diffract reference waves that provide holographic information and act as heavy atoms in the phase retrieval process, and additionally provide known structures on the silicon membrane for verification of reconstruction fidelity and spatial resolution (Fig. 3). High resolution structural information is required to fully characterize mechanical properties of these aerogels; however, many other statistical properties such as density and correlation distances can be obtained directly by standard analysis of the radially averaged small angle x-ray scattering (SAXS) patterns. We note, however, that the radially averaged raw diffraction data used in our reconstruction has a power law exponent of about -4, while diffraction patterns generated by a reconstructed 3D region containing only aerogel material reveals a power law exponent of -2 (Fig. 4), typical of the

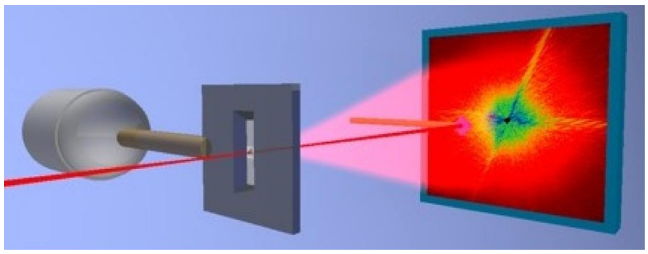

FIG. 1 (color online). Diffraction imaging layout. Coherent x rays ($\lambda = 1.65$ nm) illuminate [26,27] the sample mounted on a 50 nm thick Si_2N_3 membrane window. Diffraction patterns at various sample orientations ($+69°$ to $-64°$ in $1 \pm 0.1°$ increments) are measured using a CCD camera (20 μm pixel size, 1300×1340 pixels, 165 mm downstream). A beamstop blocks the direct beam and multiple exposure times are summed to expand the CCD dynamic range.

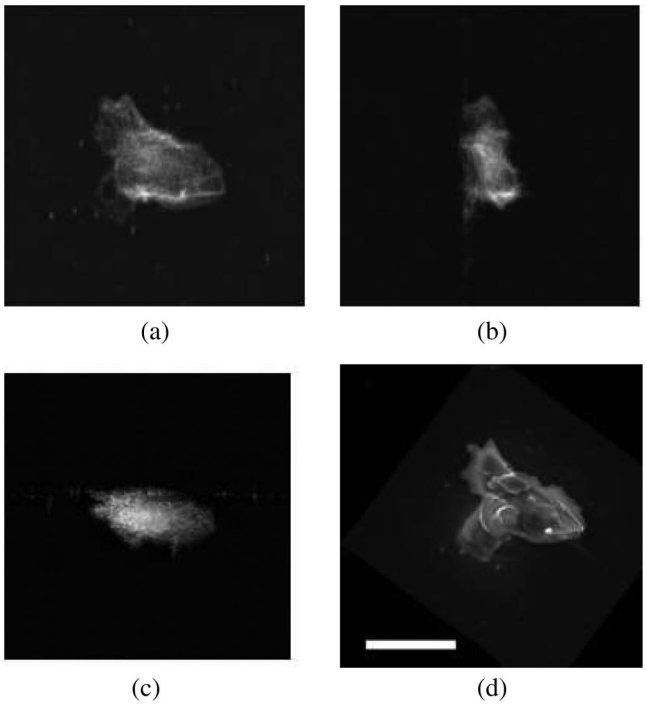

FIG. 2. (a)–(c) Orthogonal projections through the amplitude of the reconstructed 3D object. The imaged volume is 5 μm cubed with a reconstruction resolution of 15 nm. A top-down scanning electron micrograph image of the prepared aerogel sample for comparison with the 3D reconstruction is shown in (d), scale corresponds to 2 μm. Several reference platinum dots (d) are reconstructed on the membrane plane (b),(c) and the animation in supplementary materials [13].

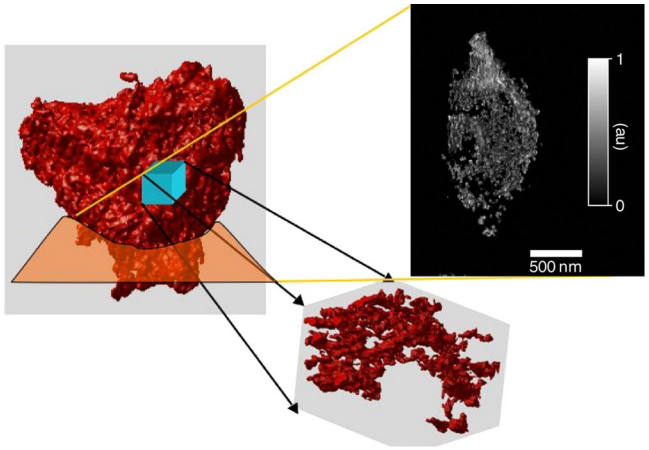

FIG. 3 (color online). Section and isosurface rendering of a 500 nm cube from the interior of the 3D volume. The foam structure shows globular nodes that are interconnected by thin beamlike struts. Approximately 85% of the total mass is associated with the nodes, and there is no evidence of a significant fraction of dangling fragments.

''string of pearls'' aerogel morphology (see below). This is because our measured data contain additional scattering from the membrane, surrounding particles and Pt contamination. These scatterers are physically separated in the 3D reconstruction, enabling scattering from just the aerogel portion of the sample to be calculated.

X-ray scattering measurements extending the spatial scales probed by diffractive imaging data were performed on a similar batch of aerogel foam at beam line 32-ID at the Advanced Photon Source (APS) [15,16]. Three distinct power-law regimes are observed at different spatial scales (Fig. 4). In the Porod region below $q \simeq 0.1$ Å^{-1} a power law with an exponent of -4 indicates that the foam has a

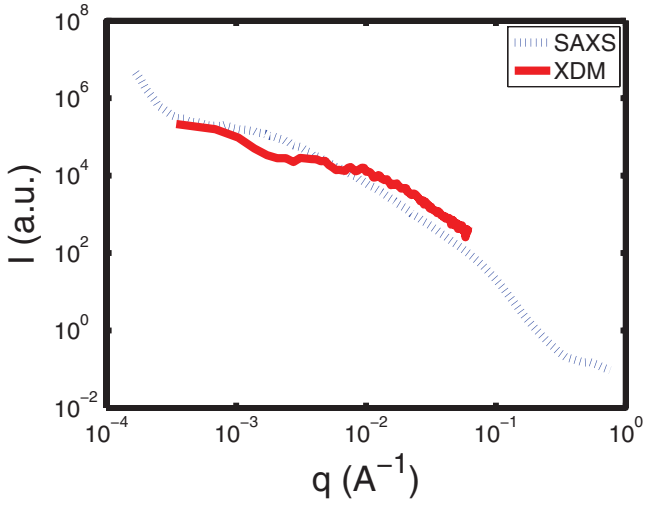

FIG. 4 (color online). Small angle x-ray scattering (SAXS) data calculated from our 3D volume reconstruction (XDM) compared to ultrasmall angle x-ray scattering measurements on a similar batch of 100 mg/cm^3 Ta_2O_5 aerogel.

smooth surface. The form factor region from $q \simeq 0.1$ Å^{-1} to $q \simeq 0.005$ Å^{-1} provides information on the shape of the individual scattering elements in the aerogel network. In this region we have a power law exponent of -2, which describes a mass fractal of dimension 2 which is consistent with a diffusion-limited cluster aggregation or the typical ''string of pearls'' aerogel morphology. Oscillations in the calculated [x-ray diffraction microscopy (XDM)] scattering are due to the size of aerogel subregion used to create the calculated plot. The crossover points between the changing slopes occur at $q_1 \simeq 0.1$ Å^{-1} and $q_2 \simeq 0.09$ Å^{-1} with an associated radii of gyration of $R_{g_1} \simeq 20$ Å and $R_{g_2} \simeq 140$ Å, respectively. Values of the power law exponents and radii of gyration are obtained by standard Porod and Guinier analysis. For aerogels a fractal analysis is commonly used to interpret the scattering data. In the fractal model R_{g_1} and R_{g_2} are related to the mean particle diameter and the correlation range, where the relation between R_g and size or correlation range depends strongly on the shapes and size distribution of the scatters. At very low q we find another power law slope associated with another scattering feature; however, the ultrasmall angle x-ray scattering data end before a clear radius of gyration is observed, therefore it is not possible to estimate the size of these structures. We can, however, limit the size of these features to more than 1 μm, the size related to the minimum scattering vector at which we still observe the power law slope behavior. Voids of several hundred nanometers are observed in the reconstructed 3D volume.

We now turn our attention to understanding the mechanical properties of these aerogels. The strength and stiffness of three-dimensional foams are often observed to scale as ρ_a^m, where ρ_a is the density of a structure divided by the density of its constituent members. In a model proposed by Gibson and Ashby [17] the scaling exponent m has limiting values of 1 where deformation is axial, and 2 for structures that deform in bending. Scaling relations in terms of ρ_a assume some degree of uniformity in the distribution of mass between the interconnecting lattice ''beams'' and the nodes that define their intersections. These assumptions appear satisfied for many foamlike structures at densities down to 10% or less ($\rho_a \lesssim 0.1$). However, the strength of many low density aerogel samples of much lower density (densities of less than 1% or $\rho_a \ll 1$) is orders of magnitude less than expected and scaling exponents between 3 and 4 are frequently observed [18,19]. Higher mass scaling exponents are attributed to the presence [20] of fragments disconnected from the load-bearing backbone structure [19], adding mass without carrying or transferring load. These disconnected fragments are a natural consequence of percolation: as a structure approaches a critical density, more of its mass becomes associated with branches disconnected from the backbone of the lattice.

It is not clear, however, that such percolation models apply to these aerogels [20,21]. In one alternative model,

heterogeneities such as micron-sized holes produce spanning structures that could fail by buckling [21]. Yet another model proposes that diffusion-limited cluster aggregation leads to fractal clusters (blobs) connected by thin beams (links) [20,22]. The response of the ''blob and link'' architecture to compressive loading is simulated with finite-element modeling, using the NIKE3D implicit finite-element solver [23]. Material data for polycrystalline tantalum oxide was used for the constitutive model with the modulus being 140 GPa. For these simulations, opposing faces are loaded in compression, while the unloaded cube faces are treated with mirror symmetry, restricting boundary motion to the plane. The average mass scaling exponent obtained by this modeling was $m = 3.6$, consistent with bulk data. When the excess node mass was removed by computational thinning, the scaling exponent reverted to $m = 2$, indicating that the primary deformation mechanism was bending of the interconnecting struts.

In this first experimental high-resolution view inside a foam, we see a structure consisting of nodes connected by thin beams. These are similar to the simulated fractal cluster aggregates and links derived from a diffusion-limited cluster aggregation model. This blob and beam structure explains why these low density materials are weaker than predicted, and explains the high mass scaling exponent observed for this material. Computational thinning of the measured structure improves the strength-to-weight ratio by orders of magnitudes, indicating that improvements in the strength could be obtained by modifying the aerogel preparation conditions in an effort to redistribute constituent material from nodes to interconnected struts. Improvements in resolution using brighter light sources, shorter wavelengths, and larger detectors would enable resolving the cross section of interconnecting struts, providing a full characterization of not only these aerogels but also a range of engineered nanoscale materials. The structural analysis we demonstrated here could be applied to other porous materials and assist modeling percolation problems such as oil and water in minerals [24,25]. More generally, the ability to image an unknown, isolated object in three dimensions at high resolution, as demonstrated here, has the potential for a wide range of applications in material science, nanotechnology, and biology at the cellular level.

This work was supported by the U.S. Department of Energy under Contract No. W-7405-Eng-48 to the University of California, Lawrence Livermore National Laboratory; Projects No. 05-SI-003 and No. 05-ERD-003 from the Laboratory Directed Research and Development Program of LLNL; the Advanced Light Source and the National Center for Electron Microscopy, Lawrence Berkeley Lab, under DOE Contract No. DE-AC02-05CH11231; the National Science Foundation through the Center for Biophotonics, UC Davis, under Cooperative Agreement No. PHY0120999. J. C. H. S. and U. W. supported by DOE Grant No. DE-FG03-02ER45996. Use of the Advanced Photon Source was supported by the U.S. Department of Energy, Office of Science, Office of Basic Energy Sciences, under Contract No. W-31-109-ENG-38.

*Corresponding author.
smarchesini@lbl.gov

[1] S. Bag *et al.*, Science **317**, 490 (2007).
[2] L. W. Hrubesh, J. Non-Cryst. Solids **225**, 335 (1998).
[3] W. L. Chao *et al.*, Nature (London) **435**, 1210 (2005).
[4] J. Miao, P. Charalambous, J. Kirz, and D. Sayre, Nature (London) **400**, 342 (1999).
[5] J. R. Fienup, Appl. Opt. **21**, 2758 (1982).
[6] D. R. Luke, Inverse Probl. **21**, 37 (2005).
[7] S. Marchesini, Rev. Sci. Instrum. **78**, 011301 (2007).
[8] J. Miao *et al.*, Phys. Rev. Lett. **97**, 215503 (2006).
[9] D. Shapiro *et al.*, Proc. Natl. Acad. Sci. U.S.A. **102**, 15 343 (2005).
[10] H. N. Chapman *et al.*, J. Opt. Soc. Am. A **23**, 1179 (2006).
[11] M. A. Pfeifer, G. J. Williams, I. A. Vartanyants, R. Harder, and I. K. Robinson, Nature (London) **442**, 63 (2006).
[12] S. Marchesini *et al.*, Phys. Rev. B **68**, 140101(R) (2003).
[13] See EPAPS Document No. E-PRLTAO-101-042830 for details on the methods. For more information on EPAPS, see http://www.aip.org/pubservs/epaps.html.
[14] C. J. Brinker and W. S. George, *Sol-Gel Science: The Physics and Chemistry of Sol-Gel Processing* (Academic, New York, 1990).
[15] J. Ilavsky, A. J. Allen, G. G. Long, and P. R. Jemian, Rev. Sci. Instrum. **73**, 1660 (2002).
[16] J. Ilavsky, P. R. Jemian, A. J. Allen, and G. G. Long, AIP Conf. Proc. **705**, 510 (2004).
[17] L. J. Gibson and M. Ashby, *Cellular Solids: Structure and Properties* (Cambridge University Press, Cambridge, England, 1997), 2nd ed.
[18] H. S. Ma, A. P. Roberts, J. H. Prevost, R. Jullien, and G. W. Scherer, J. Non-Cryst. Solids **277**, 127 (2000).
[19] R. W. Pekala, L. W. Hrubesh, T. M. Tillotson, C. T. Alviso, J. F. Poco, and J. D. LeMay, in *Mechanical Properties of Porous and Cellular Materials* (Materials Research Society, Boston, MA, 1990), Vol. 207, p. 197.
[20] H. S. Ma, J. H. Prevost, R. Jullien, and G. W. Scherer, J. Non-Cryst. Solids **285**, 216 (2001).
[21] R. Pirard and J. P. Pirard, J. Non-Cryst. Solids **212**, 262 (1997).
[22] P. Meakin, Phys. Rev. Lett. **51**, 1119 (1983).
[23] Computer code NIKE3D, in B. N. Maker, R. M. Ferencz, and J. O. Hallquist, LLNL Report No. UCRL-MA-105268, 1995.
[24] D. Stauffer, *Introduction to Percolation Theory* (Taylor and Francis, London, 1985).
[25] B. Bollobás and O. Riodan, *Percolation* (Cambridge Univeristy Press, Cambridge, England, 2006).
[26] M. R. Howells *et al.*, J. Phys. IV (France) **104**, 557 (2003).
[27] T. Beetz *et al.*, Nucl. Instrum. Methods Phys. Res., Sect. A **545**, 459 (2005).